Bioinspired Supertough Graphene Fiber through Sequential Interfacial Interactions

*Yuanyuan Zhang†, Jingsong Peng†, Mingzhu Li, Eduardo Saiz, Stephan Wolf and Qunfeng Cheng**

((† These two authors contributed equally to this work))

Dr. Y. Y. Zhang, Dr. J. S. Peng, Prof. Q. F. Cheng
Key Laboratory of Bio-inspired Smart Interfacial Science and Technology of Ministry of Education, School of Chemistry, Beijing Advanced Innovation Center for Biomedical Engineering, Beihang University, Beijing 100191, P. R. China
E-mail: cheng@buaa.edu.cn
Prof. Mingzhu Li
Key Laboratory of Green Printing
Institute of Chemistry, Chinese Academy of Sciences (ICCAS)
Beijing 100190, P. R. China
Prof. Stephan Wolf
Institute of Glass and Ceramics (WW3), Department of Materials Science and Engineering (WW), Friedrich-Alexander University Erlangen-Nürnberg (FAU), Martensstrasse 5, 91058 Erlangen, Germany
Prof. Eduardo Saiz
Department of Materials, Centre for Advanced Structural Ceramics, Imperial College London, London SW7 2AZ, U.K.

Keywords: bioinspired; graphene fibers; interfacial interactions; sequential; tough

Natural nacre exhibits extraordinary functional and structural diversity, combining high strength and toughness. The remarkable properties of nacre are attributed to i) a highly arranged hierarchical layered structure of inorganic minerals (95 vol.%) containing a small amount only of organic materials (5 vol.%), ii) abundant synergistic interfacial interactions, and iii) formation under ambient temperature. Herein, inspired by these three design principles originating from natural nacre, the supertough bioinspired graphene-based nanocomposite fibers (BGNFs) are prepared under room temperature via sequential interfacial interactions of ionic bonding and π-π interactions. The resultant synergistic effect leads to a super toughness of 18.7 MJ m^{-3} as well as a high tensile strength of 740.1 MPa. In addition, the electrical conductivity of these supertough BGNFs is as high as 384.3 S cm^{-1}. They can retain almost 80% of this conductivity even after 1,000 cycles of loading-unloading testing, which makes

these BGNFs promising candidates for application in flexible and stable electrical devices, such as strain sensors and actuators.

Natural nacre shows remarkable mechanical properties, especially high fracture toughness, due to its organic (5 vol.%)-inorganic (95 vol.%) layered architecture and the mineral bridges that penetrate the organic matrix.[1] This delicate architecture is formed under ambient temperatures with the help of abundant interfacial interactions.[1,2] Graphene-based fibers (GFs) after graphitization treatment have recently become quite enticing for promoting excellent mechanical properties and electrical conductivity.[3] For example, GFs fabricated through the wet-spinning protocol using graphene oxide (GO) after graphitization treatment have reached a high tensile strength of 2.2 GPa and high electrical conductivity of 8000 S cm^{-1}.[3a] Doping potassium (K) into GFs after graphitization can also promote electrical conductivity up to 2.24 × 10^5 S cm^{-1}.[3b] The thermal conductivity of GFs can also be significantly enhanced by graphitization.[3c] Recently, a dimensionally-confined hydrothermal strategy was developed to construct GFs with a high toughness of 30 MJ m^{-3}.[4] Another annealing treatment was also developed to achieve GFs with a high tensile strength of 724 MPa.[5]

However, graphitization usually requires an extremely high temperature (up to 3000 °C), the annealing process needs high-temperature (1200 °C) treatment, and the hydrothermal strategy also requires a temperature of more that 200 °C. These high-temperature treatments are quite harsh, expensive, and energy-intensive, hindering the large-scale fabrication of GFs. High-temperature processing also degrades some heat-labile components, most of which are the primary sources of smart functions.[4a,6]

Thus, how to design high-performance GFs under moderate temperatures still remains a great challenge. Natural materials with exceptional mechanical properties typically are assembled under ambient temperatures.[7] For example, nacre presents complex mechanisms of deformation and fracture generating high mechanical properties, particularly high fracture

toughness. This is due to its delicate design of i) layers of 'bricks' (precisely arranged aragonite crystal plates) and 'mortar' (organic materials), ii) the abundant interfaces contained within the matrix that govern the deformation and fracture of these materials, and iii) growth under moderate temperature conditions.

Nacre-inspired nanocomposite fibers based on graphene are a promising type of GF due to the fabrication process not requiring high temperatures.[8] In addition, previous works have shown that the nacre-inspired synergistic effect from different interfacial interactions between reduced graphene oxide (rGO) nanosheets significantly improves the load transfer, leading to excellent mechanical properties of BGNFs.[9] The record tensile strength of BGNFs reached by the synergistic effect is 842.6 MPa with the methods of designing covalent bonding via 10,12-pentacosadiyn-1-ol (PCDO) and ionic bonding via Ca^{2+} during the wet-spinning process.[10] The electrical conductivity of 292.4 S cm^{-1}, however, is relatively low because of the defects caused by the covalent cross-linking. Recently, the π-π interactions, or stacking, a kind of relatively strong non-covalent interplay between rGO nanosheets and other aromatic molecules, was demonstrated to be an effective approach to enhance the interfacial interactions between rGO nanosheets. This kind of interfacial interaction shows some advantages, including i) good preservation of π-conjugated domains on graphene,[11] ii) facilitation of charge transfer between aromatic molecules and graphene,[12] both benefiting the conductivity, and iii) the capability to be re-formed similar to that of sacrificial bonds,[13] resulting in promotion of toughness, and especially for the durability of loading-unloading cycles. Furthermore, the electrical conductivity retained after long-term cyclic testing. Thus, the π-π interactions are a promising approach for designing highly conductive BGNFs with excellent toughness.

Herein, inspired by the design principles originating from nacre, we developed a room-temperature fabrication process for BGNFs with excellent toughness and durability during cyclic testing through synergistic interfacial interactions of π-π interactions and ionic bonding. These BGNFs possess outstanding mechanical properties with a tensile strength of 740.1 MPa and a toughness of 18.7 MJ m^{-3}. The electrical conductivity is as high as 433.5 S cm^{-1}. In particular, the BGNFs can endure more than 1,000 cycles of loading-unloading testing without fracture and retain about 80% of the original electrical conductivity value. These multifunctional BGNFs could potentially be applied in flexible electrodes, supercapacitors, solar cells, and smart response devices.

Results and Discussion

The GO-Ca^{2+} fibers were fabricated using GO suspension with fiber thickness of ~1.0 nm (Figure S1, Supporting Information) through wet-spinning technology[10] with a coagulation bath of calcium chloride ($CaCl_2$) aqueous solution, as shown in **Figure 1**a. The ionic bonding based on Ca^{2+} was introduced during the wet-spinning process. The dried as-prepared GO-Ca^{2+} fibers were immersed into HI solution to obtain reduced GO-Ca^{2+} fibers (rGO-Ca^{2+} fibers). The further π-π interactions were formed by successively immersing pristine rGO-Ca^{2+} fibers into the N-hydroxysuccinimide ester (PSE)/dimethyl formamide (DMF) solution and 1-aminopyrene (1-AP)/DMF solution. The PSE and 1-AP could react with each other through nucleophilic acyl substitution. The combination is designated as PSE-AP. The corresponding reaction mechanism is shown in Figure S2 (Supporting Information). BGNFs obtained via the synergy of ionic bonding and π-π interactions were finally obtained, as shown in Figure 1b. The scanning electron microscopy (SEM) images of BGNFs show the aligned surface morphology and crumpled layered structure, as shown in Figure 1c-d, respectively. The as-prepared BGNFs were optimized with the addition of PSE-AP by controlling the different immersing times of PSE/DMF and 1-AP/DMF. These BGNFs are designated as BGNF-I,

BGNF-II, BGNF-III, BGNF-IV, and BGNF-V, respectively. The thermogravimetric analysis (TGA) results are shown in Figure S3 (Supporting Information), and the exact content of PSE-AP is listed in Table S1 (Supporting Information).

To verify the interfacial interactions between rGO nanosheets, fourier transform infrared spectroscopy (FTIR) was conducted, as shown in **Figure 2**a. The peaks at 1275 cm^{-1} and 1068 cm^{-1} responded to the vibration of C-N-C and N-C-O in N-hydroxysuccinimide, respectively. The peaks at 1583 cm^{-1} can be attributed to the bending of the amide N-H group.[11,14] These characteristic peaks indicate that the PSE-AP molecules successfully cross-linked the rGO nanosheets in the resultant BGNFs. The X-ray diffraction (XRD) (Figure 2b, Table S2, Supporting Information) results also show that the interlayer distance (d-spacing) of the BGNFs increases with the content of PSE-AP molecules. X-ray photoelectron spectroscopy (XPS) was further utilized to confirm the π-π interactions and ionic bonding in the BGNFs, as shown in Figure 2c. A new peak attributed to the C-N bonding at 285.8 eV appears in the C1s spectrum, indicating the introduction of the PSE-AP molecules. Two peaks which correspond to N1s (399 eV) and $Ca2p_{3/2}$ (347 eV) (Figure S4, Supporting Information), further confirm the insertion of PSE-AP and the Ca^{2+}.[10] Furthermore, the energy dispersive spectroscopy (EDS) element mapping in Figure S5 (Supporting Information) shows the existence of the N and the Ca elements,[8d,10] providing another confirmation of the synergistic modification of π-π interactions and the ionic bonding. Raman spectrum testing (Figure 2d) is also performed to characterize the π-conjugated functionalization of the PSE-AP. The relative peak intensity ratio of D band to G band (I_D/I_G) of rGO-Ca^{2+} fiber is increased from 0.95 to 1.31 for GO-Ca^{2+} fiber after HI reduction. The I_D/I_G ratio decreased from rGO-Ca^{2+} fiber to BGNF-III and BGNF-V. This decreased ID/IG ratio with the GO-pyrene interface indicates the homogenization of sp2-

hybridized carbons after the π-conjugation of pyrene groups, illustrating the π–π interaction between PSE-AP and rGO.[15]

Owing to the successful cross-linking of π-π interactions and ionic bonding between adjacent rGO interlayers, the resultant BGNFs reached excellent mechanical preparties. The typical stress-strain curves of GO-Ca^{2+} fiber (Curve 1), rGO-Ca^{2+} fiber (Curve 2), and BGNF-III (Curve 3) are shown in **Figure 3**a. The tensile strength and toughness of pristine wet-spun GO-Ca^{2+} fiber are 390.1 ± 18.5 MPa and 2.4 ± 0.4 MJ m^{-3}, respectively, which are in accordance with the previous reported results.[8d] After chemical reduction with HI, the redundant oxygen-containing groups on GO were eliminated, leading to a much more highly packed layered structure. Then the mechanical properties of the rGO-Ca^{2+} fiber were simultaneously improved to a tensile strength of 500.5 ± 10.9 MPa and a toughness of 12.0 ± 1.5 MJ m^{-3}. Impressively, after cross-linking with PSE-AP, the tensile strength and toughness of BGNF-III were enhanced dramatically to 740.1 ± 36.6 MPa and 18.7 ± 2.1 MJ m^{-3}, respectively. The stress-strain curves and exact mechanical properties of all the corresponding fibers are shown in Figure S6 and Table S3 (Supporting Information), respectively. The fracture morphology of BGNF-III shows a clear pull-out and curled edges of rGO nanosheets as shown in Figure 3b, which is different from that of the rGO-Ca^{2+} fiber with flat edges (Figure S7, Supporting Information), indicating the strong interfacial interaction between rGO nanosheets and high efficiency of load transfer onto the rGO nanosheets. The fracture morphologies of all the corresponding fibers are shown in Figure S8 (Supporting Information). During the slippage of rGO nanosheet triggered by external tensile load, the ionic bonding via Ca^{2+} firstly bears the stress and the PSE-AP molecules start to be stretched along the tensile direction. With the increase of tensile load, the ionic bonding is broken with partial load energy dissipated, and the pyrene groups on PSE-AP slide against the rGO nanosheets due to the non-covalent inherence

of π-π interactions. At this stage, the load transfer is facilitated via π-π interactions to avoid local stress concentration. Finally, the slide sites of PSE-AP are exhausted due to the growing tensile load and the π-π interactions are destroyed, leading to the fracture of the BGNF with rGO nanosheets pulled out and curved. This ionic bonding and π-π interactions between rGO nanosheets result in a synergistic effect for further improvement in mechanical properties. In addition, the π-π interactions are also good for improving the electrical conductivity for resultant BGNFs due to the facilitated charge transfer by the dipole-dipole interaction from π-π interactions.[12] Thus, the electrical conductivity with the increase of PSE-AP content is improved up to the highest value of 433.5 ± 20.7 S cm^{-1} with the PSE-AP content of 8.55 wt.% for BGNF-V, as show in Figure 3c.

BGNF-V achieved a record toughness with a high tensile strength and excellent electrical conductivity compared with other GFs fabricated under ambient temperature, as shown in Figure 3d. The gray columns represent the GFs fibers with low mechanical and electrical properties, including porous rGO fiber,[8a] rGO-chitosan,[8e] rGO-hexadecyltrimethyl ammonium bromide (GO-CTAB),[16] chemically reduced graphene-poly(vinyl alcohol) (CRG-PVA),[17] and rGO-hyperbranched polyglycerol (rGO-HPG).[18] The blue columns represent the fibers with only excellent electrical conductivity, including rGO-Ag-nanowire (rGO-Ag-NW),[19] dry graphene film scrolled,[8c] rGO-sodium deoxycholater (rGO-NaDC),[20] Writing rGO,[8b] and rGO-NaOH.[8f] The green columns stand for the fibers with good mechanical properties. These fibers include reduced giant graphene-HPG-HI (rGG-HPG-HI)[21] and large GO-sodium alginate (LGO-SA).[22] The orange columns stand for the fibers with integration of both mechanical and electrical properties, including rGG-Ca^{2+},[8d] rGO-Ca^{2+}-PCDO,[10] and the present BGNF-III. Obviously, the interfacial interaction between rGO nanosheets is vital for both mechanical properties and electrical conductivity, especially for the GFs fabricated under

ambient temperature. For example, the polymer component is usually electrically insulative and often provides weak hydrogen bonding with rGO nanosheets such as PVA,[17] chitosan,[8e] and HPG,[18] leading to both poor mechanical properties and electrical conductivities (the gray columns). The use of large-size rGG may significantly improve tensile strength and toughness with the value of 487.0 MPa and 9.5 MJ m^{-3}, respectively, but the electrical conductivity is still as poor as 52.0 S cm^{-1} due to the insulative HPG (the green columns).[21] The introduction of a highly conductive component, such as Ag-NW, can achieve a superior electrical conductivity of 930.0 S cm^{-1}.[19] But the tensile strength and toughness of rGO-Ag-NW fibers are only 300.0 MPa and 7.8 MJ m^{-3}, respectively, due to the weak interfacial interaction between Ag-NW and rGO nanosheets. Removing of insulative polymers may improve the electrical conductivity but the interfacial interactions between rGO nanosheets may be weakened, leading to poor mechanical properties, such as those of rGO-NaOH[8f] or dry graphene film scrolled[8c] (the blue columns).

To achieve integrated mechanical and electrical properties, ionic bonding is utilized for cross-linking GO nanosheets in GFs, as shown in the orange columns of Figure 3d. Xu et al.[8d] use the Ca^{2+} to cross-link large-size rGG nanosheets to obtain GFs with a tensile strength of 501.5 MPa, toughness of 16.8 MJ m^{-3}, and electrical conductivity of 410.0 S cm^{-1}. In our previous work,[10] we further added the linear molecule of PCDO to covalently cross-link rGO nanosheets with ionic bonding together. The tensile strength of GFs reaches up to 842.6 MPa. However, the toughness is only 15.8 MJ m^{-3} due to the strong confined covalent bonding without restorability. In this work, the usage of restorable non-covalent π-π interactions effectively dissipate loading energy and avoids the defects caused by the breakage of single ionic bonding. Thus, the synergistic effect from π-π interactions and ionic bonding improves the toughness up to 18.7 MJ m^{-3} among BGNFs fabricated under ambient temperature. The

tensile strength and electrical conductivity are also enhanced up to 740.1 MPa and 384.3 S cm^{-1}, respectively, illustrating the successful integration of mechanical properties and the electrical conductivity.

Another remarkable advantage of these BGNFs is the high retention rate of electrical conductivity and tensile strength after cyclic mechanical testing. As shown in **Figure 4**a, BGNF-III endured 1,000 cycles of loading-unloading testing under a maximum tensile stress of 500 MPa without fracture (Figure S9, Supporting Information). Furthermore, this BGNF could even endure 3,000 cycles of a dynamic tensile test of a maximum stress of 400 MPa and minimum stress of 250 MPa (Figure S10, Supporting Information). After 1,000 cycles of loading-unloading testing, the electrical conductivity of BGNF-III retained 78.7%, 81.6%, and 81.2% of the original value at the tensile stress levels of 500 MPa, 400 MPa, and 200 MPa, respectively (Figure 4b, Figure S11, Table S4, Supporting Information). The tensile strength retention rates of BGNF-III after 1,000 cycles are 65.0%, 64.2%, and 72.0% at the tensile stress levels of 500 MPa, 400 MPa, and 200 MPa, respectively (Figure 4b, Figure S11, Table S4, Supporting Information). Generally, no significant stress-dependent mechanical durability has been found. The conductivity retainability under different stress shows no obvious distinction, which benefits for the practical application especially under complicated stress condition. BGNF-III after 1,000 cycles of loading-unloading testing can still act as a conductive fiber to light a green light-emitting diode (LED) bulb, as shown in Figure 4c. What should be highlighted is that BGNF-III with synergistic ionic bonding and π-π interactions shows better electrical retention than the rGO-Ca^{2+} fiber. The electrical conductivity and tensile strength of rGO-Ca^{2+} fiber are retained at 68.8% and 65.5%, respectively, after 1,000 cycles at the tensile stress level of 200 MPa (Figure 4b, Figure S11, Table S5, Supporting Information).

The improvement on the durability of cyclic testing is also generated from the synergistic effect of ionic bonding and π-π interactions. Although the ionic bonding shows enhancement on interfaces under static load, the bridges via Ca^{2+} will be gradually broken under cyclic load without the ability to restore, leading to irreversible flexural deformation of rGO nanosheets and loosened layered structure (Figure 4d). In stark contrast, the introduction of π-π interactions effectively improve the stability of the layered structure during the cyclic testing (Figure 4e). As shown in Figure 4e, the random PSE-AP molecules can be aligned continuously along the tensile direction due to the continuous breaking and re-forming of π-π interactions, similar to the sacrificial bonding in the natural materials.[13,23] During this process, the π-π interactions can always transfer the loading stress between the rGO nanosheets and restrain the flexural deformation caused by the partial break of ionic bonding, until the PSE-AP molecules are all aligned. Close observation of the surface of the rGO-Ca^{2+} fiber (Figure 4f) shows that the loading-unloading cycles loosen the rGO nanosheets, resulting in lots of random ridges, which may be a key factor to impair the overlap of rGO nanosheets and increase the contact resistance. The surface morphology of BGNF-III (Figure 4g), however, still shows a highly aligned packed structure in favor of conductivity retention. In fact, synergistic interfacial interactions do improve the orientation of rGO platelets.[24]

Conclusion

In conclusion, inspired by the abundant synergistic interfaces in nacre we fabricated BGNFs via the synergistic effect stemming from ionic bonding and π-π interactions. These BGNFs have two distinct advantages: i) a fabrication process under ambient temperature and ii) superior toughness and durability during cyclic testing. The toughness of these BGNFs can reach 18.7 MJ m^{-3}, a record value among the GFs fabricated under ambient temperature. Furthermore, these BGNFs can endure more than 1,000 cycles of loading-unloading testing with a conductivity retention of about 80% under different stress levels. We believe that our

BGNFs are suitable for various practical applications from smart wearable clothing to energy devices, such as smart response devices, flexible electrodes, supercapacitors, and solar cells.

Experimental Section

Materials: GO sheets were synthesized from pure natural graphite powder by the previously reported modified Hummer's method. 57wt.% hydroiodic acid (HI) was purchased from Sigma-Aldrich. All the chemicals were used as received without further purification. 1-pyrenebutyric acid PSE and 1-AP were also purchased from Sigma-Aldrich.

Fabrication of rGO-Ca^{2+} fiber: The GO-Ca^{2+} fibers were obtained by the wet-spinning method. The spinning dope (~15 mg mL^{-1}) was loaded into a 1 mL plastic syringe with a spinning nozzle (PEEK tube with a diameter of 130 μm), and the as-prepared spinning dope was continuously injected into the rotating coagulation bath (10 rpm). The coagulation bath was an ethanol/water (1:3 V:V) solution containing 5 wt.% $CaCl_2$. The GO-Ca^{2+} gel fibers were immersed in the coagulation bath for 30 min and then transferred into the washing bath (ethanol/water solution without $CaCl_2$) to wash away the residual salts. Then the washed fibers were convolved onto the wire loop. The collected wet fibers were dried at room temperature in the air. The as-prepared dried GO-Ca^{2+} fibers were immersed into the HI solution and kept at 90 ^oC for 12 h. The container was moved out from the oven and cooled to room temperature. The fibers were washed successively by water to remove the HI and then ethanol to wash away the iodine, then dried at 100 ^oC under vacuum for 12 h in tension to achieve the rGO-Ca^{2+} fibers.

Fabrication of BGNFs: The AP and PSE were dissolved in DMF solution with 6 mM. The pristine rGO-Ca^{2+} fibers were soaked in the DMF solution of PSE at room temperature for 6 h. Then the fibers were transferred into pure DMF to remove physically absorbed PSE, and then immersed in the DMF solution containing 1-AP for 3, 6, 12, 18, and 24 h (corresponding to BGNF-I, BGNF-II, BGNF-III, BGNF-IV, and BGNF-V), followed by washing with pure DMF.

Characterization: SEM images were obtained by field-emission scanning electron microscope (JEOL-7500F). TGA was taken using NETZSCH TG 209F1 Libra, NSK under nitrogen with a temperature rising rate of 10 ^oC min^{-1}. XRD profiles were carried out with Cu-Kα radiation

(λ=1.54 nm). The mechanical properties were measured in the tensile mode using a Shimadzu AGS-X Tester at a loading rate of 0.2 mm min^{-1} with a gauge length of 5 mm. The results for each sample are based on the average value of 3~5 specimens. The cyclic testing was performed by SHENZHEN SUNS technology stock CO, LTD. at a loading and unloading rate of 0.3 mm min^{-1} with a gauge length of 5 mm. The electrical conductivities of the BGNFs were measured by a standard two-probe method using KEITHLEY 2400 Source Meter.

Supporting Information
Supporting Information is available from the Wiley Online Library or from the author.

Acknowledgements
This work was supported by the Excellent Young Scientist Foundation of NSFC (51522301), the National Natural Science Foundation of China (21273017, 51103004), the Program for New Century Excellent Talents in University (NCET-12-0034), the Fok Ying-Tong Education Foundation (141045), the 111 Project (B14009), the Aeronautical Science Foundation of China (20145251035, 2015ZF21009), State Key Laboratory of Organic-Inorganic Composites, Beijing University of Chemical Technology (oic-201701007), the State Key Laboratory for Modification of Chemical Fibers and Polymer Materials, Donghua University (LK1710), the Fundamental Research Funds for the Central Universities (YWF-16-BJ-J-09, YWF-17-BJ-J-33, YWF-18-BJ-J-13) and the Academic Excellence Foundation of BUAA (20170666) for Ph.D. Students.

Y. Y. Zhang and J. S. Peng contributed equally to this work.

References

[1] a) F. Song, A. K. Soh, Y. L. Bai, *Biomaterials* **2003**, *24*, 3623. b) U. G. Wegst, H. Bai, E. Saiz, A. P. Tomsia, R. O. Ritchie, Nat. Mater. 2015, 14, 23.

[2] a) E. M. Pouget, P. H. H. Bomans, J. A. C. M. Goos, P. M. Frederik, G. de With, N. A. J. M. Sommerdijk, *Science* **2009**, *323*, 1455; b) D. Gebauer, A. Völkel, H. Cölfen, *Science* **2008**, *322*, 1819; c) A. G. Checa, J. H. Cartwright, M. G. Willinger, *Proc. Natl. Acad. Sci. USA* **2009**, *106*, 38.

[3] a) Z. Xu, Y. Liu, X. Zhao, L. Peng, H. Sun, Y. Xu, X. Ren, C. Jin, P. Xu, M. Wang, C.

Gao, *Adv. Mater.* **2016**, *28*, 6449; b) Y. Liu, Z. Xu, J. Zhan, P. Li, C. Gao, *Adv. Mater.* **2016**, *28*, 7941; c) G. Xin, T. Yao, H. Sun, S. M. Scott, D. Shao, G. Wang, J. Lian, *Science* **2015**, *349*, 1083.

[4] a) Z. Dong, C. Jiang, H. Cheng, Y. Zhao, G. Shi, L. Jiang, L. Qu, *Adv. Mater.* **2012**, *24*, 1856; b) L. Z. Sheng, T. Wei, Y. Liang, L. L. Jiang, L. T. Qu, Z. J. Fan, *Carbon* **2017**, *120*, 17.

[5] T. Ma, H. L. Gao, H. P. Cong, H. B. Yao, L. Wu, Z. Y. Yu, S. M. Chen, S. H. Yu, *Adv. Mater.* **2018**, 1706435.

[6] a) H. B. Yao, J. Ge, C. F. Wang, X. Wang, W. Hu, Z. J. Zheng, Y. Ni, S. H. Yu, *Adv. Mater.* **2013**, *25*, 6692; b) H. Cheng, J. Liu, Y. Zhao, C. Hu, Z. Zhang, N. Chen, L. Jiang, L. Qu, *Angew. Chem. Int. Ed.* **2013**, *52*, 10482; c) H. Cheng, Y. Hu, F. Zhao, Z. Dong, Y. Wang, N. Chen, Z. Zhang, L. Qu, *Adv. Mater.* **2014**, *26*, 2909; d) C. Hu, Y. Zhao, H. Cheng, Y. Wang, Z. Dong, C. Jiang, X. Zhai, L. Jiang, L. Qu, *Nano Lett.* **2012**, *12*, 5879; e) Y. Wang, K. Bian, C. Hu, Z. Zhang, N. Chen, H. Zhang, L. Qu, *Electrochem. Commun.* **2013**, *35*, 49; f) F. Zhao, Y. Zhao, H. Cheng, L. Qu, *Angew. Chem. Int. Ed.* **2015**, *54*, 14951.

[7] a) L. B. Mao, H. L. Gao, H. B. Yao, L. Liu, H. Cölfen, G. Liu, S. M. Chen, S. K. Li, Y. X. Yan, Y. Y. Liu, S. H. Yu, *Science* **2016**, *354*, 107; b) E. Munch, M. E. Launey, D. H. Alsem, E. Saiz, A. P. Tomsia, R. O. Ritchie, *Science* **2008**, *322*, 1516.

[8] a) S. H. Aboutalebi, R. Jalili, D. Esrafilzadeh, M. Salari, Z. Gholamvand, S. Aminorroaya Yamini, K. Konstantinov, R. L. Shepherd, J. Chen, S. E. Moulton, *ACS Nano* **2014**, *8*, 2456; b) J. Cao, Y. Zhang, C. Men, Y. Sun, Z. Wang, X. Zhang, Q. Li, *ACS Nano* **2014**, *8*, 4325; c) R. Cruz-Silva, A. Morelos-Gomez, H.-i. Kim, H.-k. Jang, F. Tristan, S. Vega-Diaz, L. P. Rajukumar, A. L. Elías, N. Perea-Lopez, J. Suhr, M. Endo, M. Terrones, *ACS Nano* **2014**, *8*, 5959; d) Z. Xu, H. Sun, X. Zhao, C. Gao, *Adv. Mater.*

2013, *25*, 188; e) R. Jalili, S. H. Aboutalebi, D. Esrafilzadeh, R. L. Shepherd, J. Chen, S. Aminorroaya-Yamini, K. Konstantinov, A. I. Minett, J. M. Razal, G. G. Wallace, *Adv. Funct. Mater.* **2013**, *23*, 5345; f) Z. Xu, C. Gao, *Nat. Commun.* **2011**, *2*, 571; g) S. Gong, Q. Cheng, *Compos. Commun.* **2018**, 7, 16.

[9] a) S. Wan, J. Peng, L. Jiang, Q. Cheng, *Adv. Mater.* **2016**, *28*, 7862; b) J. Peng, Q. Cheng, *Adv. Mater.* **2017**, *29*, 1702959; c) Y. Zhang, S. Gong, Q. Zhang, P. Ming, S. Wan, J. Peng, L. Jiang, Q. Cheng, *Chem. Soc. Rev.* **2016**, *45*, 2378.

[10] Y. Zhang, Y. Li, P. Ming, Q. Zhang, T. Liu, L. Jiang, Q. Cheng, *Adv. Mater.* **2016**, *28*, 2834.

[11] H. Ni, F. Xu, A. P. Tomsia, E. Saiz, L. Jiang, Q. Cheng, *ACS Appl. Mater. Interface* **2017**, *9*, 24987.

[12] a) X. C. Dong, D. L. Fu, W. J. Fang, Y. M. Shi, P. Chen, L. J. Li, *Small* **2009**, *5*, 1422; b) B. Das, R. Voggu, C. S. Rout, C. N. R. Rao, *Chem. Commun.* **2008**, 5155; c) Y. H. Su, Y. K. Wu, S. L. Tu, S. J. Chang, *Appl. Phys. Lett.* **2011**, *99*.

[13] F. Barthelat, Z. Yin, M. J. Buehler, *Nat. Rev. Mater.* **2016**, *1*, 16007.

[14] I. W. Chen, *Chem. Commun.* **2013**, *49*, 2753.

[15] D. Zaharie-Butucel, M. Potara, A. M. Craciun, R. Boukherroub, S. Szunerits, S. Astilean, *Phys. Chem. Chem. Phys.* **2017**, *19*, 16038.

[16] H. P. Cong, X. C. Ren, P. Wang, S. H. Yu, *Sci. Rep.* **2012**, *2*, 613.

[17] L. Kou, C. Gao, *Nanoscale* **2013**, *5*, 4370.

[18] X. Hu, Z. Xu, C. Gao, *Sci. Rep.* **2012**, *2*, 767.

[19] Z. Xu, Z. Liu, H. Sun, C. Gao, *Adv. Mater.* **2013**, *25*, 3249.

[20] G. Huang, C. Hou, Y. Shao, H. Wang, Q. Zhang, Y. Li, M. Zhu, *Sci. Rep.* **2014**, *4*, 4248.

[21] X. Hu, Z. Xu, Z. Liu, C. Gao, *Sci. Rep.* **2013**, *3*, 2374.

[22] X. Hu, S. Rajendran, Y. Yao, Z. Liu, K. Gopalsamy, L. Peng, C. Gao, *Nano Res.* **2016**,

9, 735.

[23] a) S. Wan, F. Xu, L. Jiang, Q. Cheng, *Adv. Funct. Mater.* **2017**, *27*, 1605636; b) H. Huang, M. Liu, Q. Wan, R. Jiang, D. Xu, Q. Huang, Y. Wen, F. Deng, X. Zhang, Y. Wei, *Mater. Sci. Eng. C* **2018**, *91*, 201; c) J. Huang, L. Zhang, Z. Tang, B. Guo, *Compos. Commun.* **2018**, *8*, 65.

[24] S. Wan, Y. Li, J. Mu, A. E. Aliev, S. Fang, N. A. Kotov, L. Jiang, Q. Cheng, R. H. Baughman, *Proc. Natl. Acad. Sci. USA* **2018**, *115*, 5359.

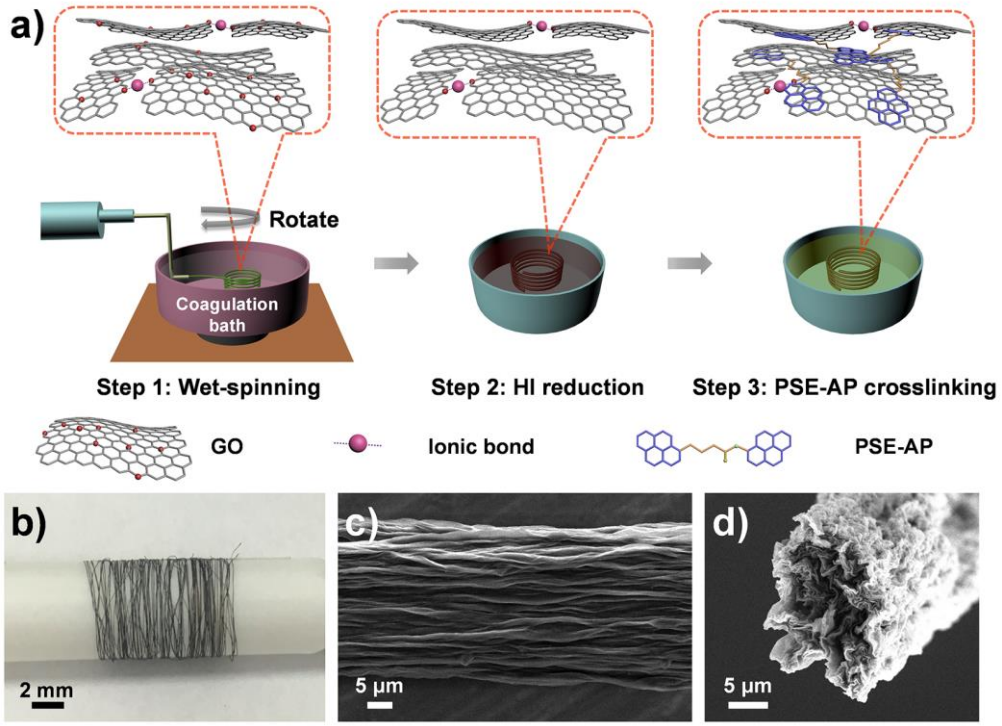

Figure 1. Schematic illustration of the fabrication process for the BGNFs. a) GO-Ca^{2+} fiber was assembled in one step by wet-spinning. After reduced by HI, the rGO-Ca^{2+} fiber was soaked into the DMF solution of PSE and 1-AP successively. b) Digital image of BGNF-III. SEM images of surface morphology c) and cross-section d) of BGNF-III, showing a regular and densely packed structure.

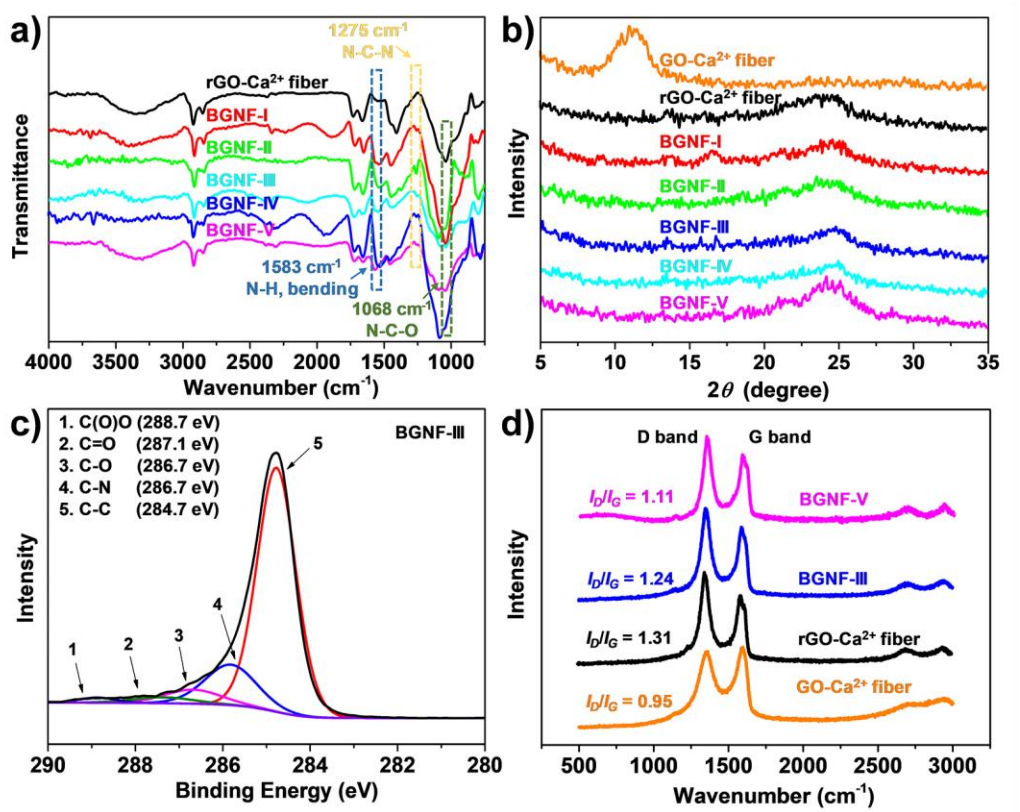

Figure 2. a) FTIR spectra of the rGO-Ca^{2+} fiber and the BGNFs. The peaks at 1275 cm^{-1} and 1068 cm^{-1} respond to the vibration of C-N-C and N-C-O in N-hydroxysuccinimide, respectively. The peaks at 1583 cm^{-1} can be attributed to the bending of the amide N-H group, indicating that the amide groups were successfully generated in the BGNFs. b) XRD spectra of GO-Ca^{2+} fiber, rGO-Ca^{2+} fiber, and the BGNFs show that the interlayer distance (d-spacing) of the BGNFs increases with the content of PSE-AP molecules, demonstrating that the cross-linked amide molecules were successfully embedded into the rGO nanosheets. c) XPS spectra of BGNF-III. The C-N peek (286.7 eV) could further indicate the introduction of PSE-AP. d) Raman spectra of GO-Ca^{2+} fiber, rGO-Ca^{2+} fiber, BGNF-III, and BGNF-V. That the value of I_D/I_G decreased from GO to rGO indicates a partial reduction of graphene. Compared with rGO-Ca^{2+} fiber, the I_D/I_G value of the BGNFs decreased slightly, verifying the restoration and homogenization of sp^2-hybridized carbons after the coverage of pyrene groups on the defect sites of rGO nanosheets.

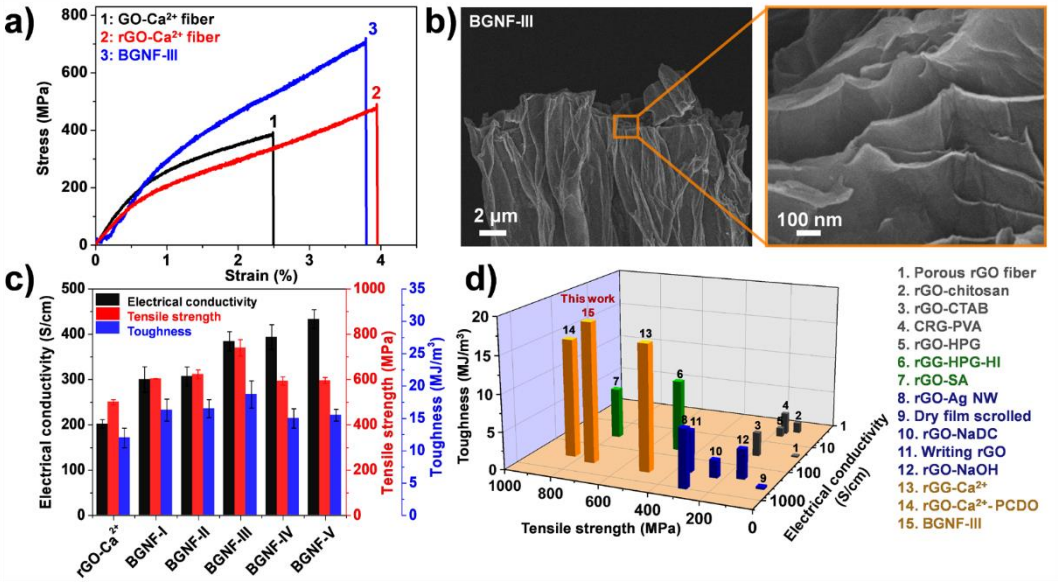

Figure 3. a) Typical stress-strain curves of GO-Ca^{2+} fiber (Curve 1), rGO-Ca^{2+} fiber (Curve 2), and BGNF-III (Curve 3). b) The rGO nanosheets of BGNF-III present the typical pullout structure and the curled edge. c) The strength, toughness, and electrical conductivity of BGNFs with different PSE-AP contents. The maximum values of tensile strength and toughness of the BGNFs appear at the PSE-AP content of 1.78 wt.%. d) Tensile strength, toughness, and electrical conductivity of BGNF-III and other graphene-based nanocomposite fibers with different tragedies at room temperature. BGNF-III's toughness is the highest of all the reported GFs assembled under room temperature to date.

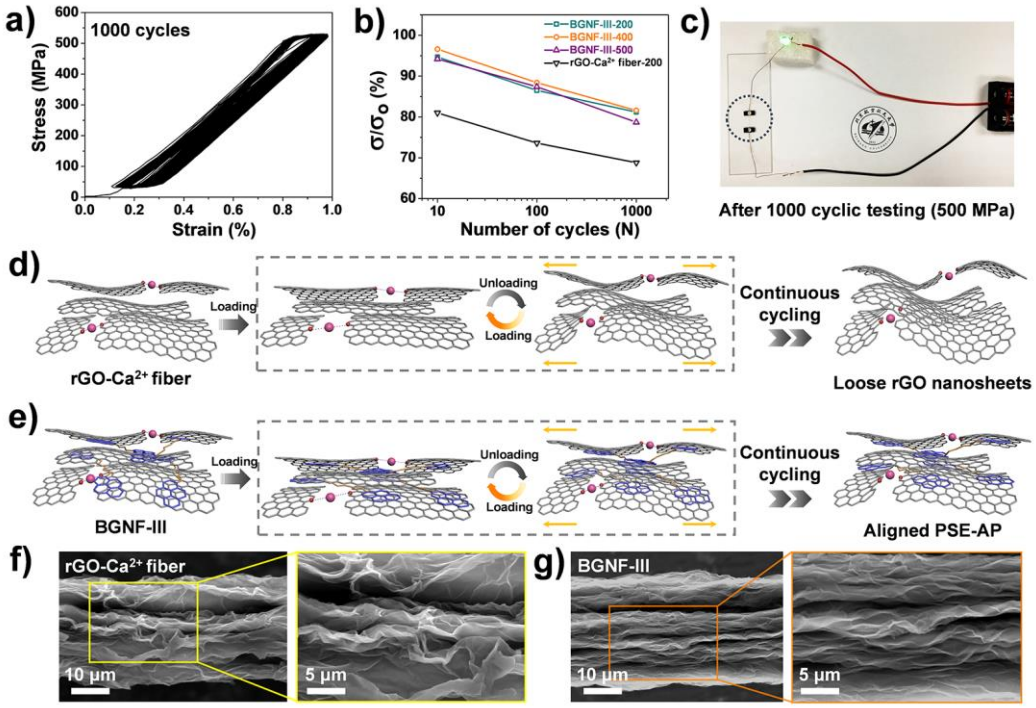

Figure 4. a) The dynamic stress-strain curve of BGNF-III under a maximum stress of 500 MPa. b) The conductivity retention of rGO-Ca^{2+} fiber and BGNF-III undergoing cyclic testing under different tensile stress. c) The nanocomposite fiber could act as a part of conductive media after1,000 cycles of loading-unloading testing. The proposed cyclic-testing mechanism of rGO-Ca^{2+} fiber (d) and BGNF-III (e). During the successive cycling test, the crack growth is restrained by the deformation-bridging process. The surface morphology of f) rGO-Ca^{2+} fiber and g) BGNF-III after 1,000 cycles.